

# Artifact-Resistant Power-Efficient Design of Finger-Ring Plethysmographic Sensors

Sokwoo Rhee\*, Boo-Ho Yang, and Haruhiko Harry Asada, *Associate Member, IEEE*

**Abstract**—A miniaturized, telemetric, photoplethysmograph (PPG) sensor for long-term, continuous monitoring is presented in this paper. The sensor, called a “ring sensor,” is attached to a finger base for monitoring beat-to-beat pulsation, and the data is sent to a host computer via a radio-frequency transmitter. Two major design issues are addressed: one is to minimize motion artifact and the other is to minimize the consumption of battery power. An efficient double ring design is developed to lower the influence of external force, acceleration, and ambient light, and to hold the sensor gently and securely on the skin, so that the circulation at the finger may not be obstructed. Total power consumption is analyzed in relation to characteristics of individual components, sampling rate, and CPU clock speed. Optimal operating conditions are obtained for minimizing the power budget. A prototype ring sensor is designed and built based on the power budget analysis and the artifact-resistive attachment method. It is verified through experiments that the ring sensor is resistant to interfering forces and acceleration acting on the ring body. Benchmarking tests with FDA-approved PPG and electrocardiogram reveal that the ring sensor is comparable to those devices in detecting beat-to-beat pulsation despite disturbances.

**Index Terms**—Ambulatory monitoring, beat-to-beat pulsation, motion artifact, plethysmograph, power consumption, ring sensor, telemetry, wearable sensor.

## I. INTRODUCTION

AS THE population of aged people increases, vital sign monitoring is increasingly important for securing their independent lives. On-line, continuous monitoring allows us to detect emergencies and abrupt changes in the patient conditions. Especially for cardiac patients, on-line, long-term monitoring plays a pivotal role. It provides critical information for long-term assessment and preventive diagnosis for which long-term trends and signal patterns are of special importance. Such trends and patterns can hardly be identified by traditional examinations. Those cardiac problems that occur frequently during normal daily activities may disappear the moment the patient is hospitalized, causing diagnostic difficulties and consequently possible therapeutic errors. Continuous and

ambulatory monitoring systems such as ambulatory electrocardiogram (EKG) are, therefore, needed to detect the trait.

The ambulatory EKG (Holter) device, one of the most widely accepted ambulatory monitoring systems, was developed and extensively studied by Holter [1]. Bellet also devised a continuous 2-hour tape recording system using a similar device [2]. When the ambulatory EKG device was first introduced, the device was not immediately widespread due to concerns over lack of documentation of coronary artery disease, reliance upon T-wave changes, and lack of recorder fidelity [3]. After many improvements and validity tests, the ambulatory EKG technology has gained increasing popularity. The ambulatory EKG, however, is not applicable to long-term monitoring for a period of several weeks or months. The machine is bulky, heavy, and uncomfortable to wear due to cumbersome wires and patches. Recently, a variety of vital sign sensors have been developed that are compact and easy to wear. Yamashita *et al.* [4] attempted to develop a simple telemetry device for monitoring pulse at a finger. This was the first attempt to implement analog photoplethysmographic (PPG) measurement on the finger base. The device can send pulse data through an analog signal transmitter. On the other hand, wristwatch-type pulse oximetry and blood pressure sensors have been developed and commercialized by several companies including Casio (BP-100 and JP200W-1V) and Omron (HEM-608 and HEM-609). These devices, although much easier to wear, have not yet been used clinically. Many technical issues still need to be solved for clinical use.

In general, long-term, ambulatory monitoring systems have not yet reached a technical level that is widely accepted by both clinicians and patients. Such long-term, ambulatory devices must be compact, lightweight, and comfortable to wear at all times. They must be designed for low power consumption for long-term use. Furthermore, they must be able to detect signals reliably and stably in the face of motion artifact and various disturbances. Unlike traditional monitoring systems, these devices are used under no supervision of clinicians. Data is collected from daily lives of patients in an unstructured environment.

The goal of this paper is to develop technology for reducing motion artifact and obtaining reliable measurements of vital signs for long-term use. A miniaturized PPG device in a ring configuration will be designed and tested. It will be shown that the device meets diverse and conflicting requirements, including compactness, motion artifact reduction, minimum loading effects, and low battery power consumption. Its benchmarking tests with FDA approved PPG and EKG will show the validity of the technology.

Manuscript received January 14, 2000; revised March 21, 2001. *Asterisk indicates corresponding author.*

\*S. Rhee is with the d'Arberloff Laboratory for Information Systems and Technology, Department of Mechanical Engineering, Massachusetts Institute of Technology, 77 Massachusetts Avenue, Room 3-351, Cambridge, MA 02139 USA (e-mail: sokwoo@mit.edu).

B.-H. Yang and H. H. Asada are with the d'Arberloff Laboratory for Information Systems and Technology, Department of Mechanical Engineering, Massachusetts Institute of Technology, Cambridge, MA 02139 USA.

Publisher Item Identifier S 0018-9294(01)05138-2.

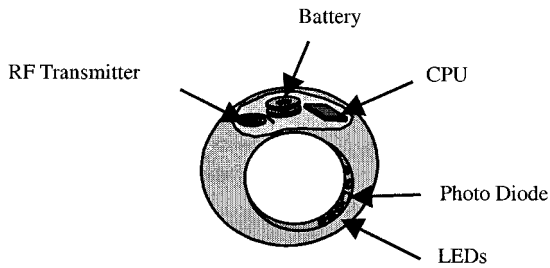


Fig. 1. Conceptual diagram of the ring sensor.

## II. THE RING SENSOR

### A. Basic Construction

The ring sensor is a miniaturized, telemetric, monitoring device worn by a patient as a finger ring. The ring encapsulates PPG, pulse oximetry combined with wireless communication and miniaturization technologies. This device optically captures the pulsation and oxygen saturation of the arterial blood flow, and transmits the signals to a host computer via a radio-frequency (RF) transmitter. Fig. 1 shows a conceptual diagram of the ring sensor [5], [6]. The ring sensor consists of optoelectronic components, a CPU, a RF transmitter, a battery, and a ring chassis. The optoelectronic components, i.e., micro photodiodes and LEDs, detect the blood-volume waveforms and oxygen-saturation level at the patient's digital artery. The CPU controls the LED lighting sequence as well as the data acquisition and transmission process. These signals are locally processed by the on-board CPU and transmitted to a host computer for diagnosis of the patient's cardiovascular conditions. The ring sensor is completely wireless and miniaturized so that the patient can wear the device comfortably 24 h/day.

This miniaturized sensor in a ring configuration is a rational design choice for 24-h continuous monitoring, since a finger ring is probably the only thing that a majority of people will be willing to wear at all times. Other personal ornaments and portable instruments, such as earrings and wristwatches, are not continually worn in daily living. When taking a shower, for example, people remove wristwatches. Bathrooms, however, are one of the most dangerous places in the home. Many thousands of people, mostly hypertensives and the elderly, die in bathrooms every year. Miniature ring sensors provide a promising approach to guarantee the monitoring of a patient at all times. Also, a ring configuration provides the anatomical advantage of having transparent skin and tissue at the finger compared with other parts of the body so that it is feasible to monitor arterial blood volume at the finger base using an optoelectronic sensor. Subsequently, a variety of simple cardiac and circulatory disorders may be detected by monitoring arterial blood volume at the finger base.

### B. Technical Issues

The ring sensor, however, is inevitably susceptible to a variety of disturbances such as a patient's motion and ambient lighting. When the patient moves, the inertia force created at his/her finger causes the ring to move relative to the skin surface, and as a result, measurement may be distorted or even ruined completely. When the ring touches an environment surface, the

contact force may cause a distortion of the measurement due to the relative displacement of the sensor to the finger. In addition, ambient lighting is another major source of artifact for optical measurement. These kinds of disturbances degrade the quality of measurement and would make the ring sensor an unreliable device.

Another important issue of this type of wearable sensor is possible necrosis of finger tissues or ulcer caused by local ischemia. To attain stable PPG signals, it is necessary to apply a certain magnitude of pressure on the skin surface. Such a pressure application is nothing harmful for short-term monitoring, but would be a problem for long-term use. With a constant, prolonged pressure at the finger base, the arteriovenous and cutaneous circulation in the finger can be obstructed, and possibly result in subsequent tissue spheclation. Numerous studies have dealt with the effect of ischemia on tissue and other types of pressure sores, and a few have addressed the critical pressure and duration problem [7]–[9]. These have found that an inverse relationship exists between the critical pressure and duration. Some also investigated the ischemic hyperemia on the finger, which may eventually result in tissue injury [10]. Therefore, the ring sensor should be designed for minimum circular obstruction by keeping the tissue pressure at a low level.

In addition, the whole electronic circuit must be designed for minimum power consumption in order to operate it for a long time without changing or recharging the battery. Among others, LED is one of the most power-consuming parts involved in the ring sensor. Therefore, the intensity of the LEDs must be lowered along with the reduction of duty cycle. This, however, incurs a poor signal-to-noise ratio problem. The signals obtained with dark LEDs are weak and must, therefore, be amplified many thousand times. As a result, it becomes susceptible to any disturbances.

There are a number of existing techniques for dealing with artifact and disturbance rejection. The most common is signal processing, as reviewed by [11]. Another standard method is to identify and reject corrupt signals by comparing pulse features with a predetermined template. Other methods use modulation by controlling the power level of multiple lighting sources [11]. All of these methods, however, involve the modification and conditioning of received signals, and do not eliminate or reduce the influence of the sources of the artifact. The artifact problem of the ring sensor is primarily due to the difficulties of attaching the sensor to the skin. This source of artifact must be removed before applying those signal processing methods.

In the following sections, a new design having a double ring configuration will be developed in order to minimize the influence of both mechanical and optical disturbances, while avoiding an excessive pressure on the finger.

## III. ARTIFACT-RESISTANT MECHANICAL DESIGN

### A. Isolating Ring Architecture

Fig. 2(a) shows the cross-sectional view of the original ring sensor where the optoelectronic sensor unit, i.e., the LEDs and photodiodes, is attached directly to the body of the ring. The problems with this design are as follows.

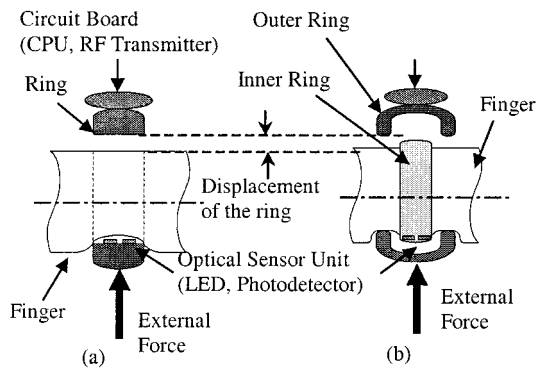


Fig. 2. Dislocation of ring sensors due to external load. (a) Traditional single-body design under external force. (b) New isolating ring sensor under external force.

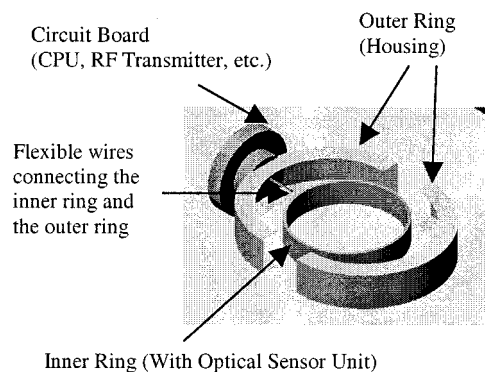


Fig. 3. Construction of isolating ring.

- When the ring touches the environment surface, the ring is pushed to one side, creating an air gap between the sensor unit and the skin, or increasing the pressure with which the sensor unit is attached. This incurs significant fluctuation in the sensor reading.
- The body of the ring sensor, including the battery and circuitry, tends to be heavy. A small acceleration of the finger and even the gravity of the ring itself may cause a displacement relative to the skin surface. Securing the ring body requires a large force applied to the finger skin.
- It is difficult to shield the sensor unit from the ambient lighting.

To resolve these problems of the original ring design, a new design is presented in this section. The new design, called a “isolating ring configuration,” is illustrated in Fig. 3. The main idea of this design is to separate the sensor unit from the rest of the ring body that is much heavier than the optical sensor unit alone. The separation is achieved by having two rings that are mechanically decoupled to each other. The inner ring shown in the figure holds the sensor unit alone, while the outer ring contains the CPU, signal processing unit, battery, and RF transmitter. Only a thin, flexible cable connects the two rings. This decoupled design has the following advantages.

*Alleviating the influence of external forces applied to the ring:* Forces due to mechanical contacts are born by the outer ring, and are not directly transmitted to the sensor unit on the inner ring. As shown in Fig. 2(b), the load of the external force is bypassed to the finger bone and is supported by the two feet

of the bridge-like outer ring. Thereby the influence of the force on the actual sensor unit attached to the inner ring inside the outer ring is alleviated.

*Alleviating the effect of acceleration on the sensor:* The inertia of the sensor unit is very small since it contains only a few LEDs and photodiodes. Due to the small inertia of the inner ring, the inertia force acting on the sensor unit is negligibly small. In consequence, the position of the optical sensor does not change significantly although the finger is accelerated.

*Reducing the skin pressure:* The outer ring does not have to be secured tightly, while the inner ring does not need a large pressure to secure the body, since it is light. Therefore, the possibility of necrosis caused by local ischemia and occlusion is lowered. This solves a critical problem for wearable sensors and long-term monitoring systems such as the ring sensor.

*Reducing the influence of the ambient lighting:* The outer ring shields the sensor unit and thereby reduces optical disturbances from the ambient lighting. The isolating ring structure provides the sensor unit with an optical shield.

Although the double ring configuration has some disadvantages such as increased size and weight, the isolation ring structure alleviates those critical problems of the original single-body ring sensor.

#### IV. POWER SAVING ELECTRONICS DESIGN

##### A. Description of the Basic Circuitry

Fig. 4 shows a block diagram of the ring sensor circuitry. The basic circuit configuration is a standard PPG circuit combined with a wireless transmitter. There are a single photodiode and LEDs of two different wavelengths, red and near infrared, involved in the circuit. The output from the photodiode is amplified and conditioned at the first stage operational amplifier. While the red and infrared LEDs are alternately turned on and off, the signal from the first stage op-amp is sampled by the two sample-and-hold circuits at different timings in order to obtain the reflected light intensity from each LED. Each channel of the signal is conditioned and converted to a digital signal with an AD converter. Using the standard RS-232 protocol, the two channels of digital signals are transmitted via a RF transmitter.

This circuit is a standard one, but the whole system is designed and operated for low-power consumption. Since the battery cell is the dominant factor determining the dimension and weight of the device, large batteries cannot be used for the ring sensor; hence, reduction of power consumption is critically important for miniaturizing the sensor. Each component has to be selected for low-power consumption and the whole system must be operated for minimum power consumption. The microprocessor coordinates the whole operation so that reliable measurement is performed with minimum power.

Unlike other simple analog devices such as the one in [4], this ring sensor uses a CPU to exploit digital control and transmission techniques in order to perform reliable and flexible operations with reduced power consumption. Digital transmission allows us to transmit multiple channels of sensor signals over the same frequency band. A variety of digital signal modulation and coding techniques can be implemented for improving RF transmission. Furthermore, power consumption can be reduced

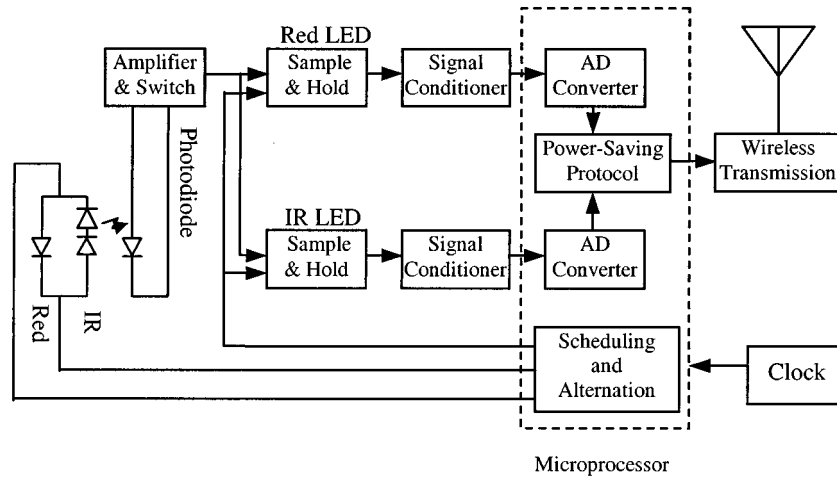


Fig. 4. Block diagram of electronic circuit.

as well. First, the duty rate of the LEDs can be controlled depending on measurement conditions. Second, data can be sent as a packet so that the RF circuitry is activated only for a short period of time. Even the whole system can be kept at a sleep mode for some period of time for further power saving. All these flexible operations are possible with use of a CPU. Use of a CPU, however, does not significantly increase the overall power consumption since the power consumed by the CPU is small (about  $100 \mu\text{A}$  with  $200 \text{ kHz}$  of clock speed) compared with the power consumed by the LED and RF transmitter.

The total power consumption depends not only on the individual component characteristics but also on the way that the whole system is controlled and operated. In the following section, a power consumption model will be derived in order to obtain guidelines for selecting components as well as for operating the system.

### B. Power Budget

Although it may vary depending on the configuration, among many components involved in the ring sensor, the LEDs and the RF transmitter consume the majority of the total power, hence, a savings in these components makes a significant contribution to the overall power saving. The objectives of this section are to provide a detailed power budget of the ring sensor, and to present an approach to minimize power consumption at the LEDs and the RF transmitter while satisfying specifications of the ring sensor. The power budget may differ depending on specific algorithms and control schemes for operating the LEDs and RF transmitter. In the following, a power budget will be obtained for a specific control algorithm that is simple and feasible to implement on a miniaturized ring sensor. For different algorithms, a power budget can be obtained without difficulty in the same way as the following formulation.

**LED:** LEDs consume a large amount of power when emitting light continuously. Therefore they must be switched on only for a short interval when light must be emitted. Namely, the LEDs must be on only when the photodiode is detecting the reflected light for measuring the pulsation. Synchronizing the sampling of the photodetector with the LED switching reduces the duty ratio of the LEDs, and thereby reduces the power

consumption. In the prototype system, this coordination is performed by the microprocessor. First, the LEDs are turned on; second, the photo detector signal is sampled at the next CPU cycle; the LEDs are switched off at the third CPU cycle. This sequence control is performed for both red and infrared LEDs. As the CPU clock cycle increases, the duty ratio of the LEDs decreases, hence, the power consumption decreases. However, the CPU consumes more power as the clock frequency increases. Therefore, a tradeoff must be made between the CPU power and the LED power in order to minimize the overall power consumption.

Key parameters associated with the LEDs' power consumption are as follows:

- $q$  internal clock frequency of the microprocessor (Hz);
- $f$  sample-and-hold frequency (Hz);
- $r$  duty ratio of LEDs;
- $C_r$  total power consumption of the red LED circuit/s;
- $C_i$  total power consumption of the infrared LED circuit/s.

In the above lighting sequence, both red and infrared LEDs are turned on for three internal CPU clock cycles, that is,  $3/q$  s. Therefore, the duty ratio of LEDs is  $r = 3f/q$ . The average power consumption of the LEDs is given by

$$P_l(q) = r(C_r + C_i) = \frac{3f(C_r + C_i)}{q}. \quad (1)$$

**Microprocessor:** In general, power consumption of a microprocessor increases with clock speed. In the prototype ring sensor, a linear relationship exists between power consumption and clock speed  $q$ :

$$P_m(q) = aq + b \quad (2)$$

where the coefficients  $a$  and  $b$  can empirically be determined.

**RF Transmitter:** The sampled analog signals are converted to digital signals by an analog-to-digital (A/D) converter and transmitted through the RF transmitter controlled by the same microprocessor. The transmission protocol is the standard RS-232 using simple on-off keying (OOK). Although there are other modulation methods, we chose OOK since it is one of the simplest schemes in terms of implementation of the circuit. The most power-consuming part of the digital RF

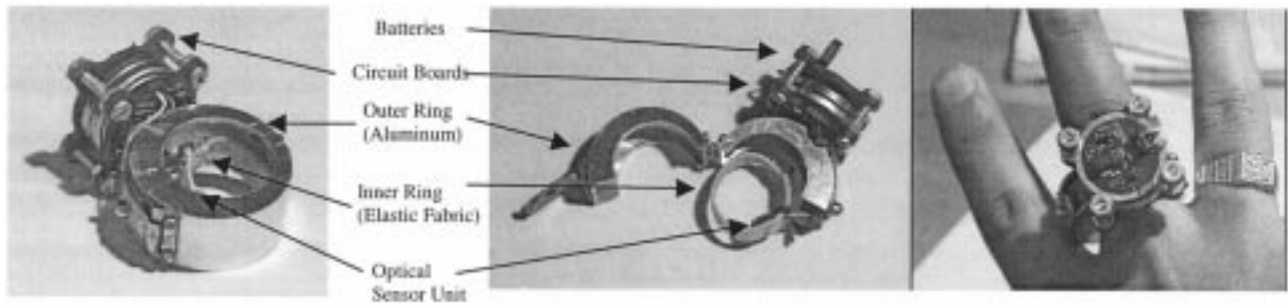


Fig. 5. Isolating ring sensor designed for motion artifact minimization.

transmitter is an oscillatory circuit involving a CMOS power transistor, which consumes a significant amount of power only when the output is high, i.e., 1 bit. In other words, the power consumption is virtually zero, when the output is low, i.e., 0 bit. Therefore, power can be saved by reducing the pulse width of each 1 bit. In the standard RS-232 protocol, the width can be reduced simply by increasing the baud rate. As the baud rate increases, transmission is completed in a shorter period of time, leaving a longer time for the transmitter to be in an idle state with no power consumption. However, a higher baud rate of the transmitter requires a higher clock frequency for the microprocessor, which results in larger power consumption. Similar to the previous case, a tradeoff must be made between the CPU power and the transmitter power. We now formulate the power budget of the transmission circuit and optimize the power consumption in terms of the clock frequency.

Key parameters associated with RF transmission are as follows:

- $d$  baud rate of transmission (bps);
- $n$  number of sample points to be transmitted/s (Hz);
- $m$  average number of high bits to be transmitted/s (bps);
- $C_t$  total power consumption of the transmission circuit/s.

Transmission of one bit needs at least six CPU instructions, including branching, port setting, carrier setting, and bit-shifting instructions. Therefore, it takes six internal CPU clock cycles. Namely, the fastest baud rate for a given clock frequency is  $d = q/6$ . In the prototype ring sensor, the resolution of the A/D converter is 8 bits in case of PIC16C711; hence, one sample point is one byte of data. Including start bit and stop bit, the standard RS-232 protocol needs five high bits to transmit on average/sample point (one byte) resulting in  $m = 5n$ . Therefore, the average duty ratio of the RF transmitter transmitting a high bit is  $m/d = 30n/q$ . The average power consumption due to RF transmission is, therefore, given by

$$P_t(q) = \frac{30nC_t}{q}. \quad (3)$$

The total average power consumption of the LEDs, RF transmitter, and microprocessor is

$$\begin{aligned} P_T(q) &= P_l(q) + P_t(q) + P_m(q) \\ &= \frac{3f(C_r + C_i)}{q} + \frac{30nC_t}{q} + aq + b. \end{aligned} \quad (4)$$

The optimal internal clock frequency  $q^*$  can be obtained by differentiating the above equation and equating it to zero

$$\frac{dP_T}{dq} = -\frac{3f(C_r + C_i) + 30nC_t}{q^2} + a = 0. \quad (5)$$

Namely

$$q^* = \sqrt{\frac{3f(C_r + C_i) + 30nC_t}{a}}. \quad (6)$$

## V. PROTOTYPING

### A. Packaging

Fig. 5 shows a prototype of the isolating ring sensor. Details of this design are as follows.

- A miniaturized sensor unit is attached to the inner ring whose mass is almost negligible. This sensor unit is a small circuit board (5 mm × 5 mm × 0.8 mm) that contains two light emitting diodes and a photodetector. As we use point-based light emitting diodes and a subminiature photodetector, this sensor unit weighs only 0.79 g.
- The main circuit board and batteries, which are heavy and bulky in comparison to the sensor unit, sit on the outer ring. The main circuitry consists of many small elements, most of which are in a surface mount or bare die form. Although the size and weight of the components used are generally small and light, the total mass of this circuit board is not negligible, 3.68 g. In addition, the button type batteries used for providing power to the circuitry are relatively heavy, 6.31 g. These components sit on the surface of the outer ring facing outward. The outer ring is made of aluminum; a block of aluminum was machined to a hollow ring as shown in Fig. 3, and all the parts other than the sensor unit were fixed to the outer ring. The thickness of the outer ring is approximately 1 mm, and the width of the outer ring is 1 cm. It is also recommended to paint the inside surface of the outer ring in black to maximize the light-shielding effect.
- The inner ring floats inside the outer ring. When a patient wears the ring, both rings are put on the same finger. Since the outer ring covers the inner ring, the external force is born by the outer ring and does not directly act on the inner ring. Although the outer ring may be dislocated due

to the external force, the sensor unit on the inner ring can be held stably, since there is no direct mechanical connection between the two rings except for a few thin wires. The thin wire is 36 AWG thick magnet wire and coated with nylon (Beldsol 8058). The two rings are mechanically decoupled.

### B. Electronic Component Selection

**LEDs and Photodiode:** One red LED and two infrared LEDs are used as the light sources. The peak wavelength of the red LED is 660 nm, and that of the infrared LEDs is 940 nm. The photodiode has the peak wavelength of 940 nm and the spectral sensitivity ranges from 500 nm to 1000 nm, which meets our needs. The voltage drop across the red LED is 1.6 V and that of the infrared LEDs is 1.2 V, and two infra-red LEDs are connected in serial. These LEDs are in a die form with a size of 0.3 mm × 0.3 mm.

**The First-Stage Amplifier:** The slew rate of the first stage amplifier must be high enough to capture the flickering LEDs, while its power consumption must be kept low. We chose OPA336 surface mount style amplifier from Burr-Brown. This amplifier has a slew rate of 0.03 V/ $\mu$ s and current consumption of 20  $\mu$ A.

**Signal Conditioner:** The signal conditioning part consists of filters and amplifiers. The signal from the first stage amplifier contains a large portion of dc signal, which is cut off by a high-pass filter. The resultant ac signal is on the order of millivolts, needing amplification on the order of 103. We used a die-form operational amplifier, MAX407, from Maxim, which consumes an extremely low current of 1.2  $\mu$ A/amplifier. Slew rate is not an important factor since the frequency of the signal in this stage is less than 10 Hz. The cutoff frequency of the low-pass filter was set to be 5 Hz.

**CPU:** The on-board CPU controls all the operations of the ring sensor, ranging from the sequence control of LED lighting and data acquisition to the conversion of analogue data to digital signals in the RS-232 format for wireless transmission. A PIC16C711 microprocessor from Microchip was selected because of its unique design for low power consumption. It consumes less than 25  $\mu$ A for 32-kHz clock frequency in the normal operation mode and almost no power consumption in the sleep mode. This CPU has 4 channels of embedded A/D converter, 13 channels of digital input–output line. It has 1 KB of EPROM that is good enough to store the whole code needed for computation. The resolution of the A/D converters are all 8-bits. In case that higher resolution is necessary, other CPUs such as PIC16C773 which has 12-bit A/D converters can be used.

**Battery:** One critical problem that is practically important is interference between the RF transmitter and the other part of the circuit. Since the RF transmitter uses OOK, the current drawn to the RF transmitter goes up and down as the output is switched between on and off. This incurs a serious fluctuation in the battery voltage and causes interference with the rest of the circuit, particularly the analog op-amps. To resolve this problem, two separate batteries were used for the prototype ring sensor: one for the RF transmitter alone and the other is for the CPU, LEDs, and op-amps. Button-type thin lithium batteries from Duracell were selected. The RF transmitter is powered with a DL2016

battery of 75 mAh rated-capacity and the CPU-LED circuit with DL2032 battery of 220 mAh rated-capacity. Both batteries have an output voltage of 3 V.

### C. The Power-Optimal Clock Frequency

Based on the power budget model obtained in the previous section and power consumption characteristics of each part selected, the optimal clock frequency for minimizing the overall power consumption will be obtained in this section. The power consumption parameters associated with the red and infrared LEDs are

$$\begin{aligned} C_r &= 2.3 \times 10^{-3} (\text{A}) \\ C_i &= 0.5 \times 10^{-3} (\text{A}). \end{aligned}$$

Note that the unit of these parameters is the ampere rather than the watt to be consistent with the battery capacity unit of ampere-hour. The CPU power consumption model, (2), was identified through experiment. The coefficients involved in the model,  $a$  and  $b$ , are given in amperes by

$$\begin{aligned} a &= 1.993 \times 10^{-9} (\text{A/Hz}) \\ b &= 6.553 \times 10^{-6} (\text{A}). \end{aligned}$$

For the prototype ring sensor, the sample-and-hold frequency was set to  $f = 1000$  Hz. The choice of this frequency depends on applications. A lower sampling frequency can be used when required accuracy is lower. The number of sample points that the RF transmitter must transmit/unit time is then  $n = 60$ . The current consumption of the transmitter circuit was identified as:

$$C_t = 4.0 \times 10^{-3} \text{ A}.$$

Substituting these parameters into (6) yields the optimal clock frequency for the CPU

$$q^* = 73.61 \text{ Hz}.$$

And the minimized current consumption is given by

$$P_T(q^*) = 0.365 \text{ mA}.$$

The other electronic components of the ring sensor include multiple op-amps, switches, sample-and-hold, and filters. The total current consumption of these components was found to be 0.126 mA. Therefore, the optimal total current consumption of the ring sensor is 0.491 mA, or 1.473 mW with 3-V batteries.

Fig. 6 shows the comparison of the power optimal design with the initial nonoptimal design. The power optimal design has reduced the power consumption to 1/7 of the original design, where  $r = 0.5$ ,  $d = 600$  bps, and  $q = 8000$  Hz. In particular, the power consumption of the RF transmitter has reduced to 1/20, while that of LEDs has reduced to 1/12. Based on these data, the battery life, i.e., the length of continuous measurement without changing the batteries, can be obtained. In the prototype ring sensor, two separate batteries are used. The RF transmitter consumes 0.098 mA in the optimal design. Therefore, the lithium battery of 75 mAh capacity can last for 31.9 days. On the other hand, the CPU-LED circuit consumes 0.393 mA, and can run continuously for 23.3 days with the lithium battery of 220 mAh. If the continuous measurement is not required, but

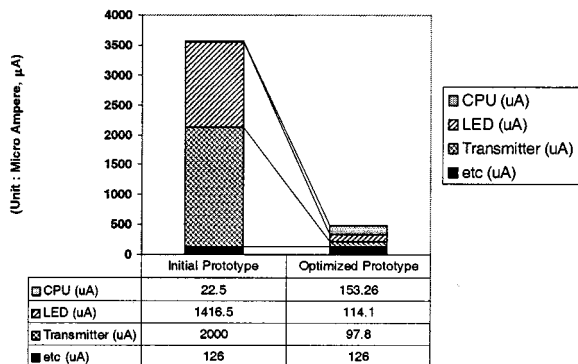


Fig. 6. Comparison of power budget.

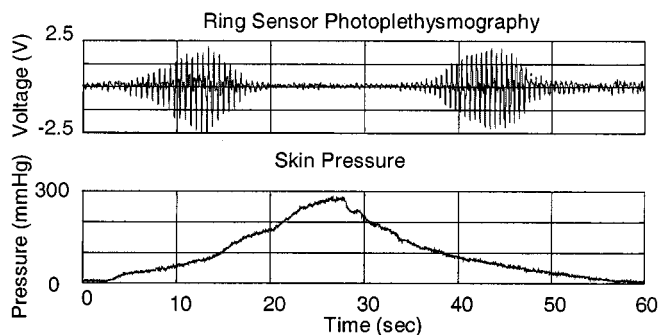


Fig. 7. Experiment of pulsation amplitude and skin pressure.

some intermittent measurement suffices, the battery life can be extended to several months to a year.

## VI. EXPERIMENT

The prototype ring sensor is now evaluated experimentally. There are several issues that need experimental verification and evaluation.

### A. Adjustment of Inner Ring Tension and Skin Pressure

The inner ring must hold the sensor unit securely and stably with an appropriate pressure against the finger skin. It is known that pressurizing the tissue increases the pulsation amplitude of blood vessels and thereby provides a better signal to noise ratio. However, as the skin pressure increases, the possibility of necrosis and blood occlusion increases. As mentioned previously, the pressure with which the sensor unit is attached to the skin must be tuned to a proper level by making a tradeoff between these two conflicting requirements.

Fig. 7 shows experiments of the skin pressure v.s. pulsation amplitude. The sensor unit of the inner ring was placed near a digital artery in order to obtain a large pulsation signal. The subject was a 29-year-old healthy male. A micro pressure gage was attached to the inner ring to measure the pressure with which the sensor unit is placed against the finger skin. The pressure was gradually increased up to 300 mm·Hg, and then gradually decreased. The pulsation amplitude measured by the ring sensor changed in accordance with the skin pressure. It increased until the skin pressure reached the 100 mm·Hg level, and then decreased. At around 180 mm·Hg, the blood vessels completely collapsed and thereby the pulsation disappeared. Although there

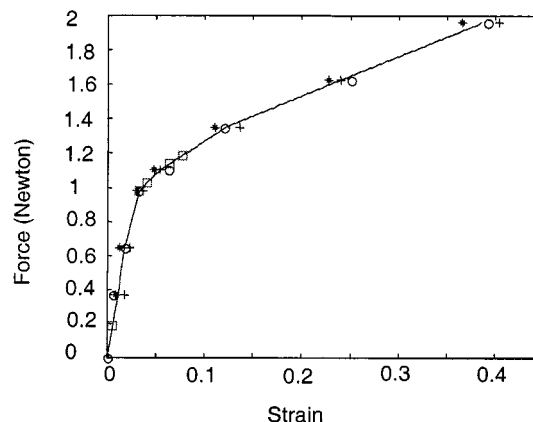


Fig. 8. Experiment of tension-strain characteristics of inner ring band. The experiments with bands with different lengths are shown as different marks.

is no published data as to the maximum allowable pressure for the finger base, literature [9] suggests that the pressure less than 90 mm·Hg causes no long-term circulation problem. We chose the skin pressure to be 75 mm·Hg, for which the amplitude is about 50% of the maximum pulsation. This amplitude is large enough to accurately measure the beat-to-beat pulsation.

The inner ring must apply this pressure and maintain the desired level despite disturbances. The thickness of the finger base, however, varies for various reasons. The inner ring must, therefore, have some compliance to accommodate the pressure in the face of variation in the finger conditions. To this end, a polyester braided elastic band (70% polyester, 30% rubber, from Rhode Island Textile Company) was used for the prototype inner ring. This has been used for underwear in the apparel industry, and proven to be comfortable to wear. This material has a unique nonlinear elasticity: the spring constant is high for small strain, while it becomes very low beyond a certain limit. Therefore, it allows the inner ring to keep the tension almost constant despite a wide range of finger diameter change.

Fig. 8 shows the experiment of the tension-strain characteristics of the polyester braided elastic band. Note that the slope is steep up to 4% of strain, i.e., high Young's modulus. Beyond this limit, the slope lowers to 1/15 of the initial steep slope. Therefore, in this range of large strain, the tension of the inner ring does not vary much, even though the finger diameter varies. In other words, the sensitivity of the inner ring tension to the finger diameter change is very low. The pressure applied to the skin surface is given by

$$P = \frac{2T}{Dw} \tag{7}$$

where

- $P$  skin pressure;
- $T$  tension;
- $D$  diameter of the elastic band;
- $w$  width of the inner ring, i.e., the elastic band.

Combining the tension-strain characteristics in Fig. 8 and the above equation, the skin pressure can be obtained based on the unsprung length of the inner ring belt and the finger diameter. This skin pressure showed a good agreement with actual measurements using the micro pressure gage.

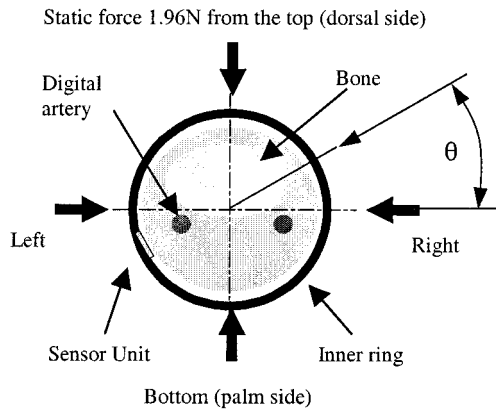


Fig. 9. Static force experiment.

### B. Comparison between the Isolating Ring and a Nonisolating Ring

To demonstrate the effectiveness of the new isolating ring sensor, several tests were conducted. First, a force was applied to the outer ring from various directions (see Fig. 9), and the pulse waveforms were measured with the isolating ring sensor, and were compared with that of the conventional single-body ring sensor. Fig. 10 shows the resultant waveforms taken from the same 29-year-old, healthy male. The top two waveforms captured by the single-body ring sensor show a significant influence of the external load. Particularly when the force is applied from the direction of  $\theta = 0^\circ$ , i.e., the opposite side of the optical sensor unit, the signal was totally destroyed due to an air gap created between the sensor unit and the skin. In this case, the optical sensor is open to the air and strong ambient light dominated the measurement. The isolating ring sensor, on the other hand, shows stable measurements despite external loads, as shown by the bottom two waveforms in the figure. The sensitivity to external loads is an order-of-magnitude lower with respect to the amplitude of the detected pulse, compared with the single-body ring sensor.

Fig. 11 shows experiments of acceleration disturbance. Pulse waveforms were recorded while the finger was shaken. As indicated along the horizontal axis, the finger was shaken for 10 s and kept stationary for the following 10 s. The process was repeated for different accelerations. The top two waveforms were taken by the single-body ring sensor under vertical ( $\theta = 90^\circ$ ) and horizontal ( $\theta = 0^\circ$ ) accelerations, respectively. Note that the waveforms are very susceptible to acceleration. The bottom two waveforms captured by the isolating ring sensor show much lower sensitivity. Even under high acceleration, the isolating ring sensor can correctly capture the basic pulse frequency. Experiments for other directions of acceleration and two-dimensional acceleration showed similar results. Although the signals are more distorted for more vigorous motion, the isolated ring sensor showed a significant improvement over the single-body sensor.

### C. Benchmarking

The new ring sensor was benchmarked with other FDA-approved devices. An EKG from AD Instruments Pty, Ltd. (NSW, Australia) and a standard fingertip PPG from IBS Corp. (MA,

USA, FDA-approved) were used for benchmarking. The three devices were attached to a subject at the same time, and data were recorded simultaneously. The fingertip PPG was attached to the tip of the middle finger of the right hand, while the ring sensor was to the base of the middle finger of the left hand. The EKG probes were attached to the standard three points of the body.

Two benchmarking tests were conducted. First, the fast Fourier transform (FFT) power spectrum of the ring sensor waveform was compared with those of EKG and the fingertip PPG. Second, the heart rate obtained from the ring sensor signal was compared with those of EKG and the fingertip PPG. Both benchmarking tests were repeated for different conditions with respect to external loads and skin pressure.

*Waveform Power Spectrum:* Fig. 12 shows the waveforms of the three devices recorded simultaneously and their FFT power spectra. The subject was the same 29-year-old healthy male. The FFT power spectra were computed for the waveform data recorded for 10 s, i.e., approximately 16 pulses. The first peak frequencies of the three spectra are exactly the same, 1.50 Hz, while the second peak around 3 Hz is within 1.6% of variation. There is no significant difference between the fingertip PPG and the ring sensor power spectra.

The ring sensor must work despite interference due to contact with the environment surface, as discussed previously. To verify that the ring sensor can function properly even under static loads, the benchmarking test was repeated with external forces applied to the ring body. Fig. 13 shows the waveforms and power spectra of the ring sensor with a static force of 1.96 N applied to the outer ring from different directions. The EKG and fingertip PPG data are shown for comparison. Note that no external load was applied to the EKG and fingertip PPG, although some variations are apparent in the finger PPG data. These variations occur when the PPG probe is detached from and reattached to the fingertip. While the amplitude of the ring sensor signal varied depending on the external load, the first and the second peak frequencies in the power spectra remained the same. The ring sensor's peak frequencies have no significant difference from those of the EKG and fingertip PPG, although the static load was applied to the ring sensor.

The skin pressure used for the above experiments was 75 mm-Hg, an acceptable pressure that will not incur local ischemia, as discussed previously. To evaluate robustness of measurement in relation to skin pressure, experiments were repeated for a low skin pressure. Fig. 14 shows waveforms and power spectra of the ring sensor when the skin pressure was lowered to 11 mm-Hg. The ring sensor still shows a consistent result with regard to the first peak frequency, although the static load of 1.96 N was applied from two directions. However, the waveforms were completely distorted when the hand was shaken. Distorted waveforms similar to the ones in the top two plots of Fig. 11 were obtained in this case. Therefore, waveforms tend to be susceptible to hand motion, as the skin pressure is lowered. As long as the ring sensor is used under stationary conditions, however, the skin pressure can be lower than 75 mm-Hg.

*Heart Rate Monitoring Tests:* The consistent detection of the first peak frequency demonstrated in the above experiments im-

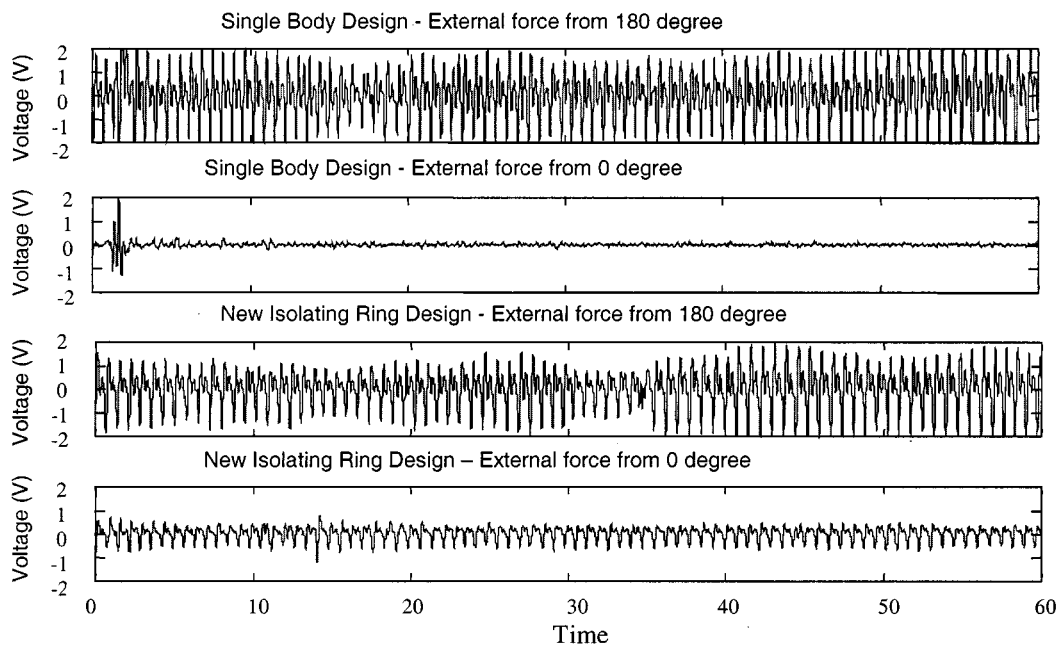


Fig. 10. Comparison between the ring sensor of single-body design and the isolating ring sensor under external static force. The initial contact pressure of isolating ring was 75 mm·Hg.

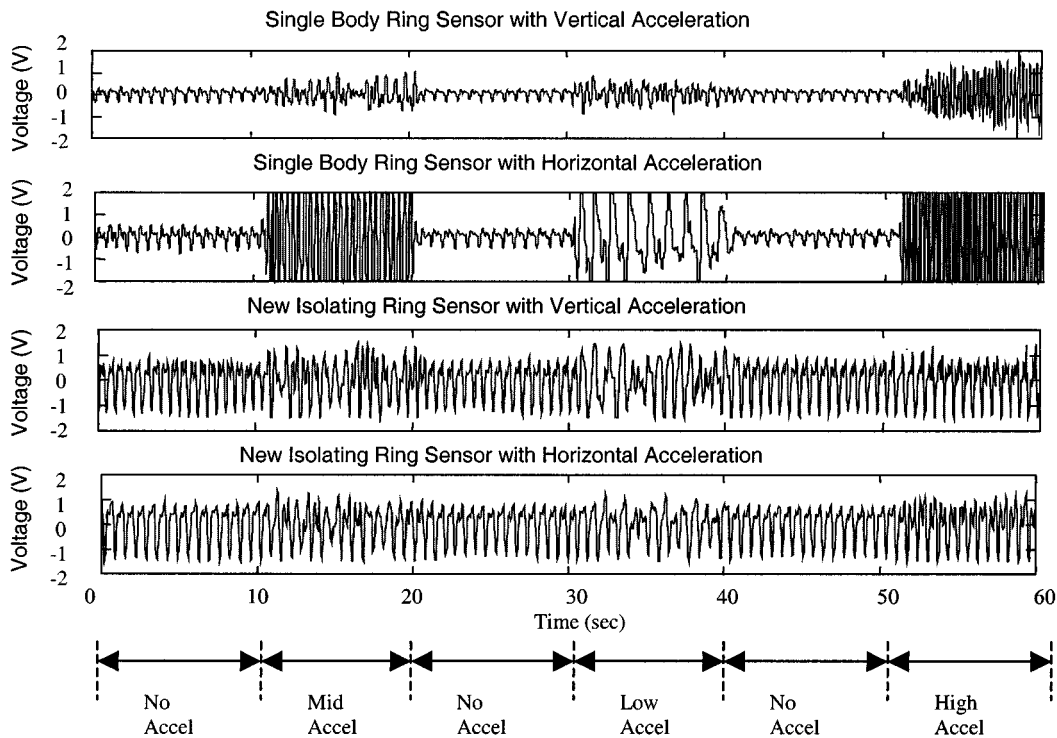


Fig. 11. Comparison between the ring sensor of single-body design and the isolating ring sensor under acceleration. The initial contact pressure of isolating ring was 75 mm·Hg.

plies that the ring sensor can be used as a beat-to-beat heart rate sensor. Fig. 15 shows the beat-to-beat heart rate measured for the same subject when a light cardiac load was applied. The heart rate was determined by detecting the base point in each pulse and measuring the interval between adjacent base points. No special software-based filtering technique was used to smooth or to reshape the waveform before detecting the base points. The result using the beat-sampling technique suggested by [12]

showed no noticeable difference from the result of this simple base point detection technique. For benchmarking, the EKG and fingertip PPG data were simultaneously recorded, and the heart rate was extracted from each signal in the standard manner of beat-sampling technique [12]. The experiment was conducted for 60 s. The variation of heart rate has close correlation with that of the EKG and fingertip PPG. Table I shows the root mean square errors (rmse) of the beat-to-beat heart rate, compared

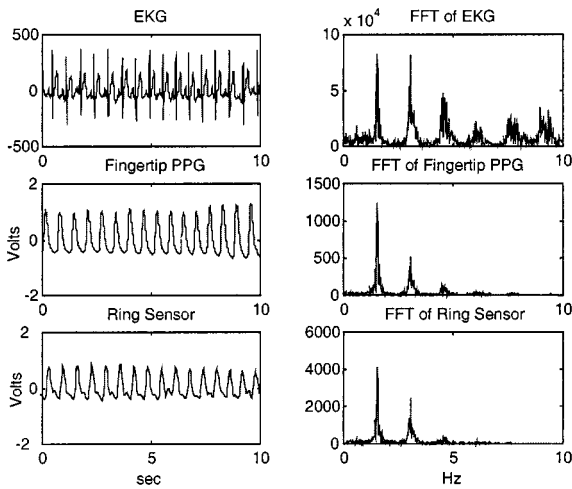
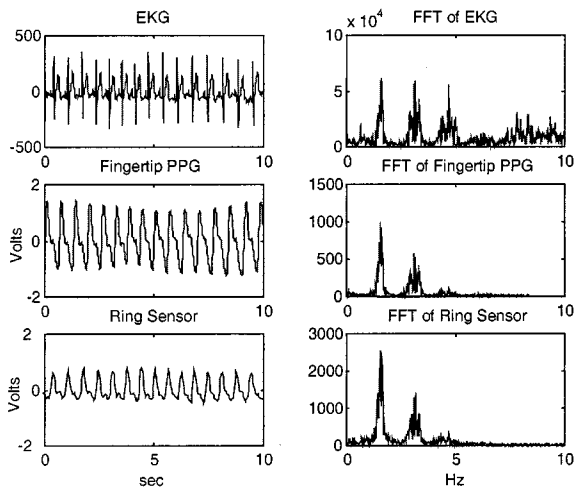
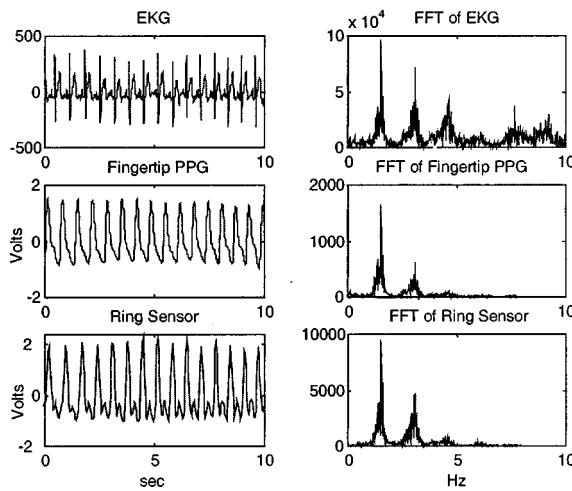


Fig. 12. No external static force with skin pressure of 75 mm-Hg. "Fingertip PPG" is the PPG at the fingertip using FDA-approved device (IBS Corp).



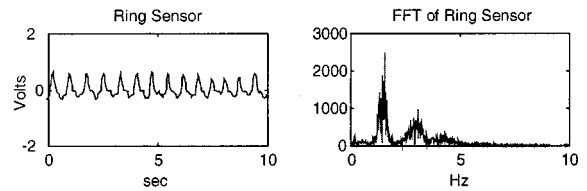
(a) Force from  $\theta = 0$  degree



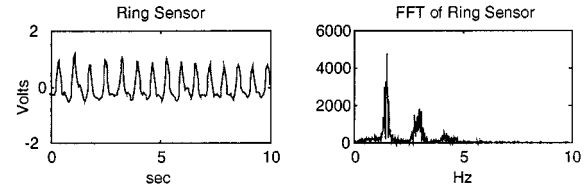
(b) Force from  $\theta = 180$  degree

Fig. 13. Static force experiment with 75 mm-Hg skin pressure. "Fingertip PPG" is the PPG at the fingertip using FDA-approved device (IBS Corp).

with the EKG and fingertip PPG. For a skin pressure of 75 mm-Hg, the difference between the ring sensor and EKG is 1.23

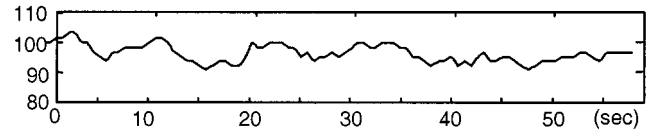


(a) Force from  $\theta = 0$  degree

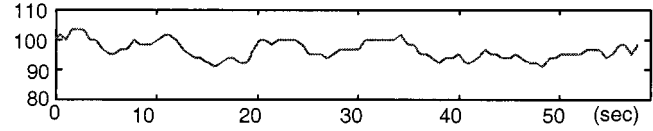


(b) Force from  $\theta = 180$  degree

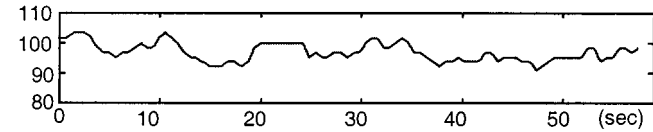
Fig. 14. Static force experiment with 11-mm-Hg skin pressure.



(a) Heart Rate (beats/min) by EKG



(b) Heart Rate (beats/in) by Fingertip PPG



(c) Heart Rate (beats/min) by Ring Sensor

Fig. 15. Heart rate monitored by EKG, Fingertip PPG device, the Ring Sensor.

TABLE I  
RMS ERROR (BEATS/MIN) OF THE HEART RATES FROM THE RING SENSOR COMPARED TO THOSE FROM EKG AND FINGERTIP PPG DEVICE

Contact pressure	EKG and Ring Sensor	Fingertip PPG and Ring Sensor	EKG and Fingertip PPG
11 mmHg	1.44	1.39	0.83
75 mmHg	1.23	1.22	0.77
137mmHg	1.41	1.27	0.96
146mmHg	1.60	1.54	0.94

beats/min, while that with the fingertip PPG is 1.22 beats/min. For comparison, the table also shows the rmse between the EKG and fingertip PPG. The discrepancy between the ring sensor and the other two is as small as that of the EKG and fingertip PPG, although some difference is noticeable. The difference of the heart rate curves such as the flat shape between 20 and 25 s in Fig. 15(c) was caused by the limited accuracy of the simple base point detection method used for the ring sensor. When the skin pressure was lowered to 11 mm-Hg or increased to 146 mm-Hg, the discrepancy tends to increase. Nevertheless, the error is as small as 1.6 beats/min.

## VII. CONCLUSION

An artifact-resistive and power-efficient design of ring sensors has been presented. The main results of this paper are as follows.

- The isolating ring design developed in this paper decouples the optical sensor unit from other components, and allows the sensor unit to be shielded from external static loads and the ambient lighting. The new ring design also attenuates the influence of finger acceleration, since the heavy components are mechanically decoupled from the sensor unit. This allowed us to hold the sensor unit with a small skin pressure, so that the circulation at the finger may not be obstructed.
- The power consumed in the ring sensor has been analyzed in relation to the characteristics of individual parts, sampling rate, transmission rate, LED lighting schedule, and CPU internal clock frequencies. Based on this power budget analysis, low-power components have been selected, power-efficient LED lighting and RF transmission methods have been derived, and the optimal CPU clock frequency has been obtained.
- A prototype ring sensor has been designed, built, and tested. Experiments have verified that the ring sensor can detect beat-to-beat pulsation in the face of interfering force and acceleration acting on the ring body. With small battery cells, the ring sensor can continuously detect and transmit plethysmograph signals for 23.3 days, while the battery life can be extended to several months with an intermittent measurement schedule.
- The prototype ring sensor has been benchmarked with FDA-approved PPG and EKG. The FFT spectral analysis has revealed that the ring sensor is comparable to the FDA-approved devices with regard to the first and second peak frequencies of the power spectra. Furthermore, the ring sensor is comparable to those devices for the measurement of beat-to-beat pulse variation. The discrepancy is less than 1.23 pulses/min in terms of the rmse.

These results clearly show that the ring sensor's accuracy is comparable to those FDA-approved devices and that the ring sensor can function even under static load and acceleration with a proper skin pressure. The ring sensor can be used as a wearable sensor for long-term, continual monitoring of patients in the home and other environments.

## REFERENCES

- [1] N. J. Holter, "New method for heart studies: Continuous electrocardiography of active subjects over long periods is now practical," *Science*, vol. 134, p. 1214, 1961.
- [2] S. Bellet, L. Roman, and J. Kostis *et al.*, "Continuous electrocardiographic monitoring during automobile driving," *Amer. J. Cardiol.*, vol. 22, p. 856, 1968.
- [3] D. David, E. L. Michelson, and L. S. Dreifus, *Ambulatory Monitoring of the Cardiac Patient*. Philadelphia, PA: Davis, 1988, ch. 1.
- [4] M. Yamashita, K. Shimizu, and G. Matsumoto, "Development of a ring-type vital sign telemeter," *Biotelemetry XIII*, 1995.
- [5] S. Rhee, B.-H. Yang, and H. Asada, "The ring sensor: A new ambulatory wearable sensor for twenty-four hour patient monitoring," presented at the 20th Annu. Int. Conf. IEEE Engineering in Medicine and Biology Society, Hong Kong, Oct. 1998.

- [6] B.-H. Yang, S. Rhee, and H. Asada, "A twenty-four hour tele-nursing system using a ring sensor," presented at the 1998 IEEE Int. Conf. Robotics and Automation, Leuven, Belgium, May 1998.
- [7] M. Kosiak, "Etiology of decubitus ulcers," *Arch. Physical Med. Rehab.*, vol. 42, pp. 19–29, 1959.
- [8] S. M. Dinsdale, "Mechanical factors in pathogenesis of ischemic skin ulcers in swine," masters thesis, Univ. Minnesota, 1970.
- [9] R. K. Daniel, D. L. Priest, and D. C. Wheatley, "Etiologic factors in pressure sores: An experimental model," *Arch. Physical Med. Rehab.*, vol. 62, pp. 492–498, 1981.
- [10] M. S. Rendell and J. M. Wells, "Ischemic and pressure-induced hyperemia: A comparison," *Arch. Physical Med. Rehab.*, vol. 79, pp. 1451–1455, 1998.
- [11] M. J. Hayes, P. R. Smith, D. M. Barnett, M. D. L. Morgan, S. Singh, and D. D. Vara, "Quantitative investigation of artefact in photo-plethysmography and pulse-oximetry for respiratory exercise testing," in *Proc. CNVD 97 Frontiers in Computer-Aided Visualization of Vascular Functions*, 1998, pp. 117–124.
- [12] J. D. Pruet, J. D. Bourland, and L. A. Gedded, "Measurement of pulse-wave velocity using a beat-sampling technique," *Ann. Biomed. Eng.*, vol. 16, pp. 341–347, 1988.



**Sokwoo Rhee** received the B.S. degree in mechanical engineering from Seoul National University, Seoul, South Korea, in 1995, and the M.S. and Ph.D. degrees in mechanical engineering from Massachusetts Institute of Technology (M.I.T.), Cambridge, MA, in 1997 and 2000, respectively.

He is currently a Postdoctoral Research Associate in the Department of Mechanical Engineering at M.I.T. His research interests include biomedical instrumentation, ultra-low power wireless communication, system analysis, and control.



**Boo-Ho Yang** received the B.S. degree in applied mathematics and physics from Kyoto University, Kyoto, Japan, in 1988, and the M.S. and Ph.D. degrees in mechanical engineering from Massachusetts Institute of Technology (M.I.T.), Cambridge, MA, in 1990 and 1995, respectively.

Currently, he is a Research Scientist in the Department of Mechanical Engineering at M.I.T. His research interests include dynamics systems and control and their applications to healthcare science and biomedical engineering problems.



**Haruhiko Harry Asada** (A'85) received the B.S., M.S., and Ph.D. degrees in precision engineering from Kyoto University, Kyoto, Japan, in 1973, 1975, and 1979, respectively.

He is Ford Professor of Mechanical Engineering and Director of the Brit and Alex d'Arbeloff Laboratory for Information Systems and Technology in the Department of Mechanical Engineering, Massachusetts Institute of Technology. He specializes in robotics, biomedical engineering, and system dynamics and control. In 1980–1981, he was a Visiting Research Scientist at the Robotics Institute of Carnegie-Mellon University, Pittsburgh, PA. He joined Department of Mechanical Engineering, Massachusetts Institute of Technology, Cambridge, MA, as a member of the faculty in 1982, and became a full Professor in 1989. His current research areas include wearable health monitoring, robotic aids for bedridden patients, human-machine interface, and multiphysics simulation.